Z. Phys. C - Particles and Fields 21, 37–52 (1983)

Zeitschrift für Physik C Particles and Fields

Particle Distribution in 3-Jet Events Produced by e^+e^--Annihilation

JADE Collaboration

W. Bartel, L. Becker, C. Bowdery[1], D. Cords, R. Eichler[2], R. Felst, D. Haidt, H. Krehbiel, B. Naroska, J. Olsson, P. Steffen, P. Warming

Deutsches Elektronen-Synchrotron DESY, D-2000 Hamburg, Federal Republic of Germany

G. Dietrich, E. Elsen[3], G. Heinzelmann, H. Kado, K. Meier, A. Petersen, U. Schneekloth, G. Weber

II. Institut f. Experimentalphysik der Universität, D-2000 Hamburg, Federal Republic of Germany

S. Bethke, A. Dieckmann, J. Heintze, K.H. Hellenbrand, R.D. Heuer, S. Komamiya, J. von Krogh, P. Lennert, H. Matsumura, H. Rieseberg, J. Spitzer, A. Wagner[4]

Physikalisches Institut der Universität, D-6900 Heidelberg, Federal Republic of Germany

A. Bell[5], A. Finch, F. Foster, G. Hughes, T. Nozaki, H. Wriedt

University, Lancaster, England

J. Allison, J. Baines, A.H. Ball, R.J. Barlow, J. Chrin, I.P. Duerdoth, I. Glendinning, F.K. Loebinger, A.A. Macbeth, H. McCann, H.E. Mills, P.G. Murphy, P.G. Rowe, K. Stephens

University, Manchester M13 9PL, England

D. Clarke, R. Marshall, G.F. Pearce, J.B. Whittaker

Rutherford Appleton Laboratories, Chilton, Didcot, Oxon OX11 0QX, England

J. Kanzaki, T. Kawamoto, T. Kobayashi, M. Koshiba, M. Minowa, M. Nozaki, S. Odaka, S. Orito, A. Sato, H. Takeda, T. Takeshita, Y. Totsuka, S. Yamada

Lab. of Int. Coll. on Elementary Particle Physics and Department of Physics, University of Tokyo, Japan

Received 13 September 1983

Abstract. We have studied the distribution of particles within and between jets of 3-jet final states produced in the reaction $e^+e^-\to$hadrons at c.m. energies of 22 GeV and 29–36.4 GeV. The lowest energy jet shows distributions of transverse momenta, particle flow, and energy flow which differ significantly from those of the other two jets and from jets of 2-jet events at $E_{cm}=14$ GeV. First order QCD calculations with subsequent fragmentation of quarks and gluons into hadrons indicate that the lowest energy jet has the largest probability of originating from a gluon. To reproduce the observed differences in an independent parton fragmentation model, the secondary quarks of a gluon jet have to have higher transverse momenta and lower parallel momenta than those of a quark jet. The particle densities between the jets as well as the correlation of transverse and longitudinal momenta of the particles within the jets favour models with fragmentation along the colour axes.

1. Introduction

Hadron production by high energy electron positron annihilation is well described by models based on perturbative QCD with subsequent fragmentation of the quarks and gluons. In the majority of events, the hadrons show a clear 2-jet structure with an angular distribution of the jet axes as predicted for the process $e^+e^-\to q\bar{q}$. The angle and energy distributions

1 European Science Exchange Fellow
2 Now at Labor f. Hochenergiephysik der ETH-Zürich, Villigen, Switzerland
3 Now at SLAC, California, USA
4 Heisenberg Foundation Fellow
5 Now at British Petroleum, London, England

of 3-jet events are well reproduced by the inclusion of gluon bremsstrahlung [1] $e^+e^- \to q\bar{q}g$. Furthermore, evidence was recently reported for a 4-jet structure [2] as expected from higher order diagrams.

An important further step in testing QCD is to identify the gluon jet and to unravel its structure. This might be achieved by a detailed analysis of the jet-structure, since high energy gluon jets are predicted [3] to differ from quark jets of the same energy, as a result of the 3-gluon coupling and the larger colour charge of the gluon. However, at the e^+e^- energies presently available, the distributions of particles within a jet are dominated by nonperturbative effects which tend to obscure the differences between quark jets and gluon jets predicted by QCD.

The present paper summarizes several searches for such differences using data taken with the JADE-detector at PETRA. Because of the complexity of the hadronic final state, it is difficult to unambiguously define and compare jets. Nevertheless, by comparing the data with detailed model calculations which are based on lowest order perturbative QCD but use different fragmentations for quarks and gluons, it is found, that the particle distribution within the jets yields evidence for gluon fragmentation different from that of quarks. For this purpose the global properties of jets are investigated (such as transverse and longitudinal momentum distributions, particle multiplicities and energy flow) which are compared with the different model calculations. In particular we study whether 3-jet data are better described by schemes with partons fragmenting independently of each other, or by colour string models. It is shown that these two extremes differ in the predicted particle distributions in the angular region between the jets, as well as in the particle distributions within the jets. First results of these investigations have been published in [4, 5].

The present analysis uses $e^+e^- \to$hadrons data obtained at centre-of-mass energies of 14 GeV, 22 GeV and in the region between 29 and 36.4 GeV (centering at 33 GeV) with the JADE-detector at the e^+e^--storage ring PETRA. The criteria for selecting the events and the definition of jets are described in Chap. 2, the model calculations in Chap. 3, and the experimental results are presented and compared with model expectations in Chap. 4.

2. Event Selection

A description of the detector, the trigger conditions and the selection of hadronic events is given in [6]. For the present analysis the data are grouped into three energy bins as listed in Table 1. The criteria for the selection of 3-jet events which are the same as in [4, 5] will be repeated here for completeness.

Table 1. The total number of events used in the analysis for the three c.m. energy regions. The number of '3-jet' and 'planar 3-jet' events as defined in the text are also listed

E_{cm}(GeV)	14	22	29.5–36.4
$\langle E_{cm}\rangle$(GeV)	14	22	33.4
Total number of events	2,739	1,945	18,424
Number of 'planar 3-jet' events	149	228	2,048
Number of '3-jet' events	354	359	2,566

Events are classified according to their shape in momentum space using the eigenvalues of the sphericity tensor

$$T_{\alpha\beta} = \sum p_{i\alpha} \cdot p_{i\beta} / \sum p_i^2, \tag{1}$$

where $p_{i\alpha}$ is the α-component ($\alpha = x, y, z$) of the momentum of the i-th particle. The summation is over all charged particles with momenta above 100 MeV/c and over all neutral particles with energies above 150 MeV. The momenta of neutral particles are determined from the energy deposited in the lead glass counters, assuming the observed neutral particles to be photons. For charged particles penetrating one or more lead glass clusters, the average energy deposited in the lead glass by a minimal ionising track was subtracted from the cluster energy. If the remaining energy was less than 150 MeV no photon was introduced. For each event the sphericity tensor (1) is constructed and diagonalized. In the analysis its normalized eigenvalues Q_1, Q_2, Q_3 ($Q_1 < Q_2 < Q_3$) and the corresponding principal axes $\mathbf{q}_1$, $\mathbf{q}_2$, $\mathbf{q}_3$ of the momentum ellipsoid are used. An event plane is defined by ($\mathbf{q}_2, \mathbf{q}_3$). Figure 1 shows the event distribution of the 33 GeV sample in the Q-plot. Most of the events are of the 2-jet type and thus cluster at large $Q_3 - Q_2$ values. Planar events are defined by the cuts: $Q_1 < 0.06$ and $Q_2 - Q_1 > 0.07$, as indicated in Fig. 1.

For each planar event the particles are attributed to one of the three jets which are obtained by maximizing the triplicity [7],

$$T_3 = (|\sum_{n_1} \mathbf{p}_i| + |\sum_{n_2} \mathbf{p}_i| + |\sum_{n_3} \mathbf{p}_i|) / \sum_{\text{all}} |\mathbf{p}_i| \tag{2}$$

where n_1, n_2 and n_3 are three nonintersecting sets of particles.

Caution is required in relating kinematic parameters such as total energies and directions of jets to the corresponding ones of partons. Partons and jets have different invariant masses and the '4-vector' of a jet is not identical to that of the parton which

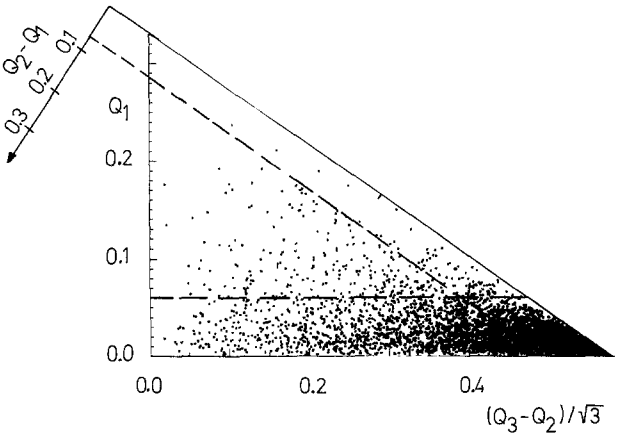

Fig. 1. The Q-plot as defined in the text using the data of the E_{cm} $=33$ GeV sample. The lines indicate the cuts $Q_1<0.06$ and $Q_2-Q_1>0.07$

gave rise to the jet. For each event the jet energies are calculated by employing two different methods: The jet energy E_j^e is defined as the sum of the particle energies within a jet j, assuming charged particles to be pions and neutral ones to be photons.

$$E_j^e=\sum_{i=1}^{n_j} E_{i,j} \quad (j=1,2,3) \tag{3}$$

n_j = number of particles in jet j;
$E_{i,j}$ = energy of i^{th} particle in jet j.

In the second method the jet energies E_j^d are calculated from the jet directions $\mathbf{k}_j$ which are given by the vector sum of the particle momenta within each jet. This procedure is strictly applicable only in the case of three massless jets.

$$E_j^d=\frac{\sin\Theta_{k,l}}{\sin\Theta_{1,2}+\sin\Theta_{2,3}+\sin\Theta_{3,1}}\cdot E_{cm}; \quad (j,k,l \text{ cyclic}) \tag{4}$$

$\Theta_{k,l}$ = angle between the jets k and l projected onto the event plane $(\mathbf{q}_2,\mathbf{q}_3)$.

Note that even for an ideal detector, E_j^d and E_j^e do not coincide, since, at present energies, jet masses are not negligible in comparison with jet total energies.*

The three jets are ordered using E_j^d, according to:

$$E_1^d>E_2^d>E_3^d. \tag{5}$$

Events with jets which contain less than 4 particles, or which have $E_j^e<2$ GeV, are rejected. The events surviving these cuts are called 'planar 3-jet' events.

* The observed average jet mass is roughly given by 0.35 E_j^e for all three jets in the region 4 GeV $<E_j^e<15$ GeV

The number of events available at the different c.m. energies is listed in Table 1.

The lowest energy jet of 3-jet events at E_{cm} $=33$ GeV is similar in energy to those in 2-jet events at $E_{cm}=14$ GeV. The latter ones are used for comparison because they should mainly consist of quark jets. The 2-jet events are taken from the data recorded at $E_{cm}=14$ GeV, without applying any cuts in the Q-plot. For each event the particles are divided into two jets by the plane perpendicular to the sphericity axis $\mathbf{q}_3$. The two jet directions $\mathbf{k}_j$ are given by the vector sum of the particle momenta within the jets. The event is rejected if $|\cos(\mathbf{k}_1,\mathbf{k}_2)|$ is less than 0.9, if one jet contains less than 4 particles, or if one energy $E_j^e<2$ GeV. Both jets (4170 in total) of an accepted event are used in the analysis.

Whereas 2-jet events are not restricted by any cut in the Q-plot, for 'planar 3-jet' events the event shape distribution normal to the $(\mathbf{q}_2,\mathbf{q}_3)$-plane is influenced by the cut $Q_1<0.06$. To be less affected by this cut in the comparison with 2-jet events an enlarged sample of '3-jet' events is defined by $Q_1>0.06$ *or* $Q_2-Q_1>0.07$, excluding only the 2-jet corner.

3. Model Calculations

To some extent the jet definitions given above are arbitrary and different definitions will yield somewhat different jet directions and energies. Any comparison of observed distributions with QCD predictions must take into account these definitions and procedures. The present investigation uses model calculations to study how well primordial quark and gluon momenta can be reconstructed and how different gluon fragmentation schemes modify the average final state hadron configuration. From the bremsstrahlung-like energy spectrum of the gluon in the process $e^+e^-\to q\bar{q}g$, one expects that the lowest energy jet (#3) has the highest probability of containing the gluon fragments. This behaviour is confirmed by model calculations.

The calculations start from parton configurations given by first-order QCD. Since the $q\bar{q}g$ cross section diverges when the $q\bar{q}$-configuration is approached, the total cross section is separated into 2-jet and 3-jet contributions:

$$\sigma_0(1+\alpha_s/\pi)=\sigma_{q\bar{q}}+\sigma_{q\bar{q}g} \tag{6}$$

$$\alpha_s=12\pi/(33-2n_f)\ln(s/\Lambda^2).$$

The quark gluon coupling strength α_s was calculated taking $\Lambda=0.3$ GeV [8] and $n_f=5$. The separation of $q\bar{q}$ and $q\bar{q}g$ processes is achieved in regions of phase space where the final hadron configuration of $q\bar{q}$

and $q\bar{q}g$ events are practically indistinguishable. Two fragmentation schemes were studied to describe the conversion of quarks and gluons into hadrons. The two schemes differ in the treatment of $q\bar{q}g$ events.

One scheme assumes that quarks, antiquarks and gluons fragment independently, as expected if the jet evolution is correctly described by parton branching processes down to small off-shell masses and if long range nonperturbative effects play a minor role. In the actual application of this scheme we take a more phenomenological approach by using the model of Hoyer et al. [9] (Hoyer model), where the jet evolution is parametrized according to Field and Feynman [10]. In the overall c.m. system the distribution of the transverse momenta of the secondary quarks relative to the primary quark direction is

$$d\sigma/d^2p_\perp \sim \exp(-p_\perp^2/2\sigma_{q,q}^2). \tag{7}$$

In the case of gluon fragmentation $\sigma_{q,q}$ is replaced by $\sigma_{q,g}$. The sum of energy and longitudinal momentum $E+p_\parallel$ of the hadrons is distributed according to a fragmentation function

$$f(z)=\begin{cases}1-a_q+3a_q(1-z)^2; & a_q\leqq 1\\ (1+a_q)(1-z)^{a_q}; & a_q\geqq 2.\end{cases} \tag{8}$$

For the gluon fragmentation a_q is replaced by a_g. Gluons are treated as quark-antiquark pairs but the gluon momentum is carried entirely by one of the quarks, which subsequently fragments. To test how sensitive the observed distributions are to different gluon fragmentations, the values of $\sigma_{q,g}$ and a_g are taken either to be the same as for primary quarks (the resulting distributions being denoted by $g=q$) or chosen differently (denoted by the changed parameters). The following parameters were used: a production ratio of secondary u, d, and s quark pairs of 3:3:1, equal fraction of pseudoscalar and vector mesons, $\sigma_{q,q}=330\,\text{MeV}$ and $a_q=0.5$ for the light quarks and $a_q=0.0$ for the heavy ones.

The second scheme is the Lund model [11], in which fragmentation proceeds along the colour flux lines. For $q\bar{q}g$-events these flux lines connect quark and antiquark via the gluon as intermediary. The model is formulated in terms of strings and, although the gluon is considered as one unit, the model is kinematically equivalent to a treatment of the gluon as a collinear quark-antiquark pair $(q',\bar{q}')$ with the momentum shared equally between q' and $\bar{q}'$. Each of the two 'gluon pieces' forms a $q\bar{q}'$ or $q'\bar{q}$ two-jet system with the primary $\bar{q}$ or q. In the $q\bar{q}'$ and $q'\bar{q}$ rest frames the hadrons within these jet systems are distributed as in simple two-jet systems, a special treatment being made only for the leading hadron at the gluon corner. For more details see [11]. The parameters are the same as for quarks in the first scheme except for the fragmentation function which is replaced by $f(z)=(1+\beta)(1-z)^\beta$ with $\beta=0.4$ for the light quarks and $\beta=0.1$ for heavier ones.

The parameters of both the Hoyer model, and the Lund model have been adjusted to yield reasonable agreement not only for the 3-jet data, but also for the overall data sample. The effects of baryon production, which has been incorporated into the Lund model, are negligible for the present analysis.

The model calculations discussed so far are limited to the process $e^+e^-\to q\bar{q}$ and $q\bar{q}g$. We checked the influence of including '4-parton' events from second order terms of hard gluon radiation [11, 12]. Of course, some of the '4-parton' events are due to the gluon selfcoupling and should lead to a different behaviour of the gluon jet. 4-parton final states were generated (requiring the masses of all possible parton pairs to exceed 5 GeV), and allowed to fragment. These '4-parton' events were then subjected to the above 3-jet analysis to estimate their contribution to differences between quark and gluon jets.

Monte Carlo techniques were used to calculate the four-momenta of the final state particles. The four-momenta, including those of bremsstrahlung photons from the initial leptons, [13], were then converted into the actually measured quantities, such as drifttimes, pulse heights etc., taking the imperfections of the apparatus into account. These simulated events were processed by the same chain of computer programs as the data and were selected according to the same cuts.

For a comparison of these model calculations with the experimental data we refer to Chap. 4. Here we present the results of some resolution and efficiency studies using these calculations. In particular the question to what extent the reconstructed jet directions $\mathbf{k}_j$ reflect the original parton directions was studied and whether the lowest energy jet #3 does preferentially have the gluon direction. Regarding these questions the differences between the two fragmentation schemes turn out to be small and we present the results of the Hoyer model only.

Figure 2a shows the distribution of the angle δ between $\mathbf{k}_j$ and the closest parton direction, obtained for planar $q\bar{q}g$ events generated at $E_{\text{cm}}=33\,\text{GeV}$. On average, the spread of δ is larger for jet #3 than for #2 and #1. This is due to the fact that jet #3 has the lowest energy. In Fig. 2b the average value of δ, plotted as a function of E_j^e, is seen to follow a universal curve $\sim 1/E_j^e$ for all three

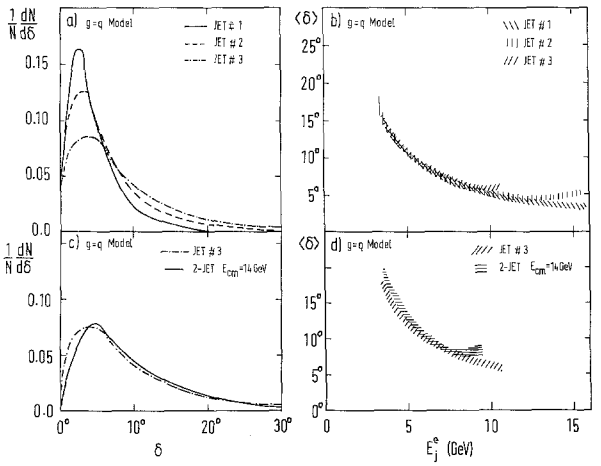

Fig. 2a–d. Prediction of fragmentation models. **a** The distribution of the angle δ between the reconstructed jet direction $\mathbf{k}_j$ and the closest parton direction for the three jets, obtained for planar $q\bar{q}g$ events generated at $E_{cm}=33$ GeV. **b** The average value of δ as a function of the jet energy. The width of the shaded areas indicates the statistical errors. **c** The distribution of the δ for jets of 2-jet events at $E_{cm}=14$ GeV together with that for jet #3 of the 3-jet' events at $E_{cm}=33$ GeV. **d** The average value of δ as a function of jet energy for the two samples used in **c**

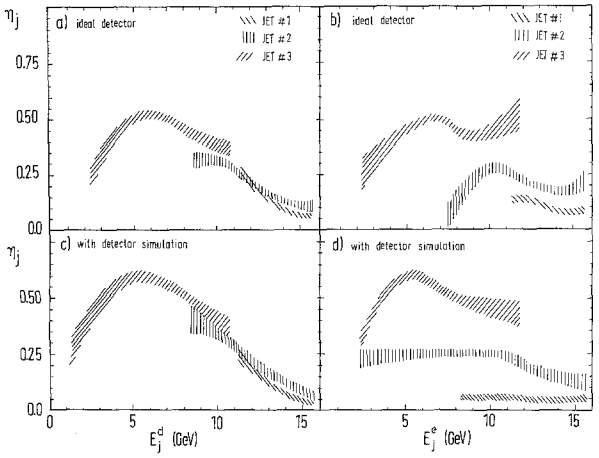

Fig. 3a–d. Prediction of fragmentation models. The probabilities η_j for jet j being closest to the gluon direction as a function of E_j^d (for **a** and **c**) and of E_j^e (for **b** and **d**) obtained from modal calculations at fixed c.m. energy of 33 GeV, assuming an ideal detector (**a** and **b**). and simulating the known imperfections of the detector (**c** and **d**). The width of the shaded areas indicates the statistical errors

jets. Without showing the curves we mention that in the Lund model the points for jet #3 lie slightly above those of #2 and #1. Figure 2c shows the distribution of δ for 2-jet events at $E_{cm}=14$ GeV together with the corresponding distribution for jet #3 of the '3-jet' events at $E_{cm}=33$ GeV. In Fig. 2d $\langle\delta\rangle$ is plotted as a function of E_j^e. These results suggest that the distribution of the jet direction around the parton direction depends mainly on E_j^e.

For the assignment of jets to partons, we use the smallest angle between the parton momentum and the jet directions. At c.m. energies of 33 GeV the probability for jet #1, #2, and #3 being closest to the gluon direction is 12%, 22%, and 51%, respectively, at 22 GeV the corresponding values are 9%, 20% and 34%. The sum of these probabilities does not add up to 100%, the remaining 3-jet structures are faked by $q\bar{q}$-events. Figures 3a and b show the probabilities η_j for jet j being closest to the gluon direction as a function of E_j^d and E_j^e, respectively, obtained from model calculations at a fixed c.m. energy of 33 GeV and assuming an ideal detector. The decrease of η_3 at jet energies below 5 GeV is due to the increasing portion of residual $q\bar{q}$-events.

In order to establish differences between quark and gluon jets, it is of special interest to compare jets of similar energies but of different gluon content η_j. On the average jet #3 has the largest gluon content but Fig. 3a shows only a small overlap between E_2^d and E_3^d and within this overlap region only small differences between η_2 and η_3. This behaviour is a consequence of the fact that (4) and (5) are used in the determination of E_j^d and in the definition of jet number j as well. By kinematics the region of overlap extends from $E_{cm}/4$ to $E_{cm}/3$, independently of how well or badly E_j^d reproduces the parton energy. Therefore the condition $E_2^d \approx E_3^d$ preferentially selects events exhibiting 2-fold symmetry around $\mathbf{k}_1$, for which jet #2 and #3 have equal probability of being a gluon. On the other hand as shown in Fig. 3b, the overlap region and the difference in gluon content are considerably larger, if E_j^e is taken as energy scale and (4) and (5) are used only to determine j. In Figs. 3c and d the corresponding probabilities η_j are drawn with the simulation of the detector effects included. The same trends as in Figs. 3a and b are visible. Jet energies of $E_2^e < 7$ GeV and $E_1^e < 11$ GeV in Fig. 3d are due to the imperfections of the detector (jets with $E_1^e < 8$ GeV are rejected).

In order to obtain a large overlap region and different values for η_j, using E_j^d, a data sample containing events from different c.m. energies is required. The comparison is then made between jet #3 at high E_{cm} and jet #2 at lower E_{cm}. With either definition for E_j we have looked for differences between the particle distribution of quark and gluon jets of the same energy.

In the following analysis frequent use is made of jets $j=2,3$ with $6\,\text{GeV} < E_j < 10\,\text{GeV}$. In this energy range the model calculations show that for both E_j^e (for the 33 GeV sample) and E_j^d (for 22+33 GeV

sample) the gluon content in jet #2 is about 25% and in jet #3 about 50%.

4. Results

In this section we present the distribution of the transverse and longitudinal momentum with respect to the jet axis, particle and energy flow within jets and perform a comparison between different jets. Three different methods are used to compare jets of about the same energy but different gluon content.

– The first one uses planar 3-jet events at $E_{cm} \sim 33$ GeV taking E_j^e as energy scale.
– The second one also includes the data at $E_{cm} = 22$ GeV and uses E_j^d as energy scale, so that the comparison is done mainly between the lowest energetic jet of high E_{cm} and the medium one of lower E_{cm}.
– Finally the jets #3 at $E_{cm} \sim 33$ GeV are compared with 2-jet events at $E_{cm} = 14$ GeV.

To check for possible biases, the same comparisons are performed with the various model calculations. At the end of this section we demonstrate that the data prefer one fragmentation scheme over the other.

All results shown are observed distributions which have not been corrected for any acceptance etc. Only statistical errors are quoted and shown in the figures. The systematic uncertainties are highly correlated between the jets and should largly cancel if appropriate ratios of measured quantities are considered.

4.1. Transverse Momentum

a) 3-jet Events. For the experimental data sample at $E_{cm} = 33$ GeV, Fig. 4a shows the average transverse momentum for the sum of charged and neutral particles within a jet j relative to the jet axis $\mathbf{k}_j$ for all three jets as a function of E_j^e. The data clearly indicate that at a given E_j^e, jet #3, the one preferentially created by the gluon, shows a larger $\langle p_\perp \rangle$ than jet #2 and jet #1. As a quantitative measure of the effect, the ratio:

$$r_{32} = \frac{\langle p_\perp \rangle_{j=3}}{\langle p_\perp \rangle_{j=2}} \tag{9}$$

was determined for each energy bin and then averaged for the range $6\,\text{GeV} < E_j < 10\,\text{GeV}$. The value obtained as well as its statistical error is listed in the first row of Table 2. To estimate the systematic uncertainties, $\langle p_\perp \rangle_j$ was calculated applying different cuts and particle selection criteria. The resulting

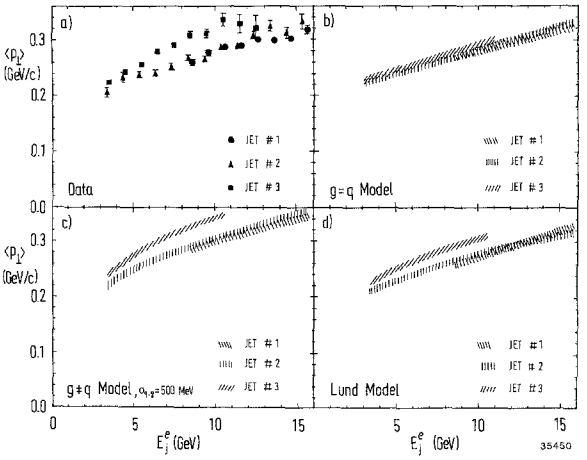

Fig. 4a–d. The average transverse momentum of charged and neutral particles within a jet relative to the jet axis for the three jets as a function of E_j^e for **a** the experimental data, and **b**, **c**, **d** for different model results at $E_{cm} = 33$ GeV

$\langle r_{32} \rangle$ values, some of which are listed in Table 2, rows 2–7, were found to be the same within the statistical errors.

To ensure that the observed effect is not caused by a bias due to the jet selection procedure we show in Figs. 4b–d and Table 2 the $\langle p_\perp \rangle$ distributions and $\langle r_{32} \rangle$ values predicted by the models. For the $q=g$ model ($\sigma_{q,q} = \sigma_{q,g} = 330$ MeV) the $\langle p_\perp \rangle$ of all three jets follows nearly a universal curve (Fig. 4b) and $\langle r_{32} \rangle$ is found to be close to 1. The observed different behaviour of jet #3, however, is qualitatively reproduced if we increase $\sigma_{q,g}$ to 500 MeV (Fig. 4c and Table 2) or if we use the Lund model (Fig. 4d). Even the inclusion of second order QCD terms does not improve the disagreement with the $g=q$ model. Feeding only '4-parton' events into the above 3-jet analysis, we find a small increase of $\langle p_\perp \rangle$ for all three jets, but the enhancement of jet #3 relative to jet #2 and #1 is less than for example that in Fig. 4d. The resulting value of $\langle r_{32} \rangle$ for these '4-parton' events alone is 1.07 ± 0.03. Furthermore, we expect at most 20% of our 3-jet event sample to be due to '4-parton' events.

The average transverse momentum $\langle p_\perp^{out} \rangle$ normal to the event plane shown in Fig. 5 as a function of E_j^e also indicates a broader $p_\perp$ distribution of jet #3, an observation which is not simple to explain in the colour string model based on first order QCD.

In Fig. 6a $\langle p_\perp \rangle$ is plotted against E_j^d instead of E_j^e, including data down to $E_{cm} = 22$ GeV, and in Figs. 6b–d the same is done for the different models. Similar tendencies as in Fig. 4 are present, as also seen from the corresponding $\langle r_{32} \rangle$ given in row 1 of Table 3.

The differential distributions of the transverse

Table 2. The ratio $\langle r_{32}\rangle$ of $\langle p_\perp\rangle$ of the lowest energy jet to $\langle p_\perp\rangle$ of the medium energy jet for different particle and event selection criteria. $\langle r_{32}\rangle$ represents an average of the 4 bins covering the range $6\,\text{GeV}<E_j^e<10\,\text{GeV}$. Row 1 gives the ratio for the data shown in Fig. 4a. Row 2 shows this ratio for charged particles only; row 3 for particles exceeding an energy of 0.5 GeV, row 4 for particles within a 50° cone around the jet axis, and row 5 for particles pointing into the hemisphere towards the highest energy jet. The ratios in rows 6 and 7 include all particles, but include only those events for which the total energy agrees within 20% with E_{cm} (row 6) or for which the angle between $\mathbf{q}_1$ and the beam direction is less than 70° (row 7). The ratio given in row 8 is obtained from the data shown in Fig. 5a. The corresponding ratios are also given for the model predictions. The errors quoted are the statistical ones

Row	Variables used in $\langle r_{32}\rangle$	Further cuts	Data	$\langle r_{32}\rangle=\left\langle\frac{\langle p_t\rangle_{j=3}}{\langle p_t\rangle_{j=2}}\right\rangle$; $[6\,\text{GeV}\leqq E_j^e\leqq 10\,\text{GeV},\ E_{\text{cm}}=33\,\text{GeV}]$			
				Lund model	Hoyer et al. $\sigma_{q,q}=330\,\text{MeV}$, $a_q=0.5$		
	p_t				$\sigma_{q,g}$ a_g	330 MeV 0.5	500 MeV 0.5
1	$p_\perp$		1.16 ± 0.02	1.10 ± 0.02		1.03 ± 0.02	1.13 ± 0.02
		particle cut:					
2	$p_\perp$	charged only	1.18 ± 0.02	1.10 ± 0.02		1.04 ± 0.02	1.15 ± 0.02
3	$p_\perp$	$E_{ij}>0.5\,\text{GeV}$	1.17 ± 0.02	1.10 ± 0.02		1.04 ± 0.02	1.12 ± 0.02
4	$p_\perp$	$\sphericalangle(\mathbf{p}_{ij},\mathbf{k}_j)\leqq 50°$	1.16 ± 0.02	1.10 ± 0.02		1.03 ± 0.02	1.13 ± 0.02
5	$p_\perp$	$\sphericalangle(\mathbf{p}_{ij},\mathbf{k}_1)<\sphericalangle(\mathbf{k}_j,\mathbf{k}_1)$ (projected onto $(\mathbf{q}_2,\mathbf{q}_3)$	1.16 ± 0.02	1.10 ± 0.03		1.02 ± 0.02	1.14 ± 0.03
		event cut					
6	$p_\perp$	$0.8\leqq\frac{\sum_{j=1}^{3}E_j^e}{E_{\text{cm}}}\leqq 1.2$	1.14 ± 0.03	1.10 ± 0.03		1.00 ± 0.03	1.13 ± 0.03
7	$p_\perp$	$\cos(\mathbf{q}_1,\mathbf{z})\|>0.35$	1.17 ± 0.02	1.09 ± 0.03		1.04 ± 0.02	1.15 ± 0.02
8	$p_\perp^{\text{out}}$		1.16 ± 0.02	1.09 ± 0.02		1.01 ± 0.02	1.12 ± 0.02

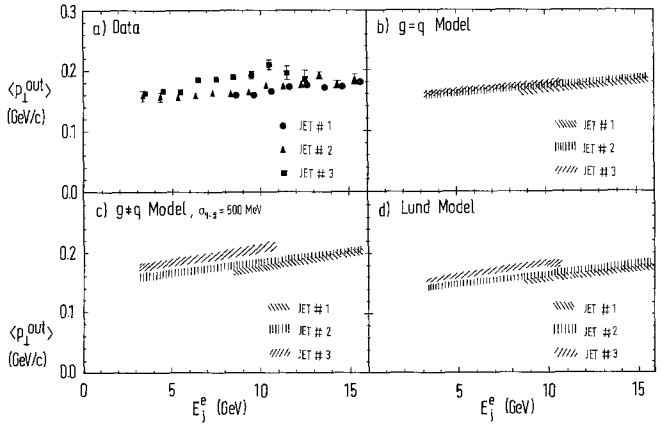

Fig. 5a–d. The average transverse momentum of the particles normal to the event plane $(\mathbf{q}_2, \mathbf{q}_3)$ as a function of E_j^e, for **a** the experimental data, and **b**, **c**, **d** for different models at $E_{\text{cm}}=33$ GeV

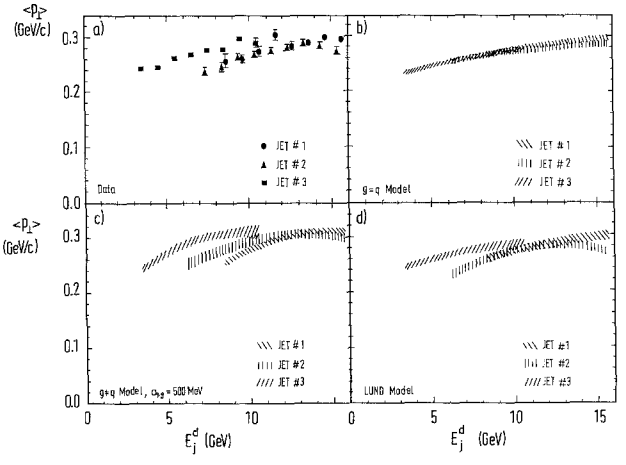

Fig. 6a–d. The average transverse momentum of the particles as a function of E_j^d using the 22+33 GeV sample for **a** the experimental data, and **b**, **c**, **d** for different models

momenta are shown in Fig. 7, for jet #2 and #3 of $6\,\text{GeV}<E_j^e<10\,\text{GeV}$ in Fig. 7a, and of $6\,\text{GeV}<E_j^d<10\,\text{GeV}$ in Fig. 7b. Both charged and neutral particles are included in these distributions which are normalized to the number of jets. The data points between $0.2\,\text{GeV}<p_\perp<1.5\,\text{GeV}$ are well described by an exponential

$$d\sigma/dp_\perp\sim\exp(-A_j p_\perp) \tag{10}$$

as indicated by the lines in Fig. 7. The best fits yield a ratio $A_2/A_3=1.18\pm0.03$ for Fig. 7a and $A_2/A_3=1.13\pm0.04$ for Fig. 7b confirming in both cases $\langle p_\perp\rangle$ to be significant larger for jet #3. Including charged particles only the corresponding ratios are

Table 3. The ratio $\langle r_{32}\rangle$ of $\langle xx\rangle$ of the lowest energy jet to $\langle xx\rangle$ of the medium energy jet for different definitions of xx. $\langle r_{32}\rangle$ represents an average of the 4 bins covering the range $6\,\text{GeV} < E_j^d < 10\,\text{GeV}$ from the 22+33 GeV sample. Row 1 gives the ratio for $p_\perp$; row 2 for $p_\parallel$, row 3 the ratio for charged and neutral multiplicity per jet and row 4 the ratio for charged multiplicity only. The corresponding ratios are also given for the predictions of the Lund model and the Hoyer model with different values of the parameters $\sigma_{q,g}$ and a_g for the gluon

Row	xx	$\langle r_{32}\rangle = \left\langle \frac{\langle xx\rangle_{j=3}}{\langle xx\rangle_{j=2}} \right\rangle$; $[6\,\text{GeV} \leqq E_j^d \leqq 10\,\text{GeV}\ \ E_{cm} = 22+33\,\text{GeV}]$						
		Data	Lund model	Hoyer et al. $\sigma_{q,q}=330\,\text{MeV}$, $a_q=0.5$				
				$\sigma_{q,g}$	330 MeV	330 MeV	500 MeV	500 MeV	500 MeV
				a_g	0.5	1.0	0.5	1.0	4.0
1	$p_\perp$	1.13±0.02	1.08+0.02		1.01+0.02	1.02+0.02	1.10+0.02	1.07+0.02	1.08+0.02
2	$p_\parallel$	0.94±0.04	1.01+0.02		1.08+0.02	0.99+0.02	1.17+0.02	1.05+0.02	1.01+0.02
3	n	1.06+0.02	1.03+0.02		0.93+0.02	1.03+0.02	0.87+0.02	0.95+0.02	0.97+0.02
4	n_{ch}	1.07+0.02	1.03+0.02		0.96+0.02	1.03+0.02	0.81+0.02	0.99+0.02	1.02+0.02

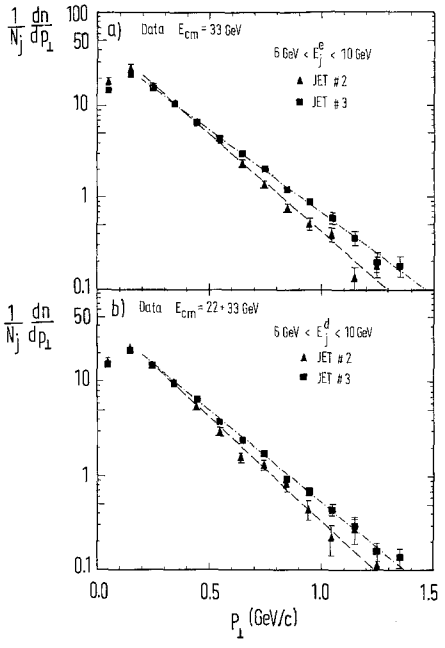

Fig. 7a and b. The differential $p_\perp$-distribution of charged and neutral particles for jets #2 and #3 with $6\,\text{GeV} < E_j < 10\,\text{GeV}$ from the 33 GeV data sample **a** and from the 22+33 GeV data sample **b**. N_j=number of jets in the defined energy region. The lines represent exponential fits to the data

$A_2/A_3 = 1.22 \pm 0.04$ and $A_2/A_3 = 1.10 \pm 0.05$, respectively.

b) Comparison with 2-jet Events. The hypothesis of a broader gluon fragmentation, causing a broader distribution of jet #3, can also be tested by comparing the properties of jet #3 with jets of similar energy from 2-jet events. As already stated in Chap. 2, we use the enlarged sample of '3-jet' events. (This enlargement of the data sample leaves the results of the previous section essentially unaltered, the main difference being a higher 4-parton event fraction. The $\langle r_{32}\rangle$ for this sample is 1.16±0.02.) The average energy of jet #3 from the 33 GeV data sample is similar to the average jet energy of the 2-jet events from the 14 GeV sample, as evident from Table 4 where the various $\langle E_j\rangle$ are listed.

Table 4. The average jet energies (E_j^d and E_j^e) for jets #1, #2, and #3 for '3-jet' events at $E_{cm}=33\,\text{GeV}$ and the same for jets from 2-jet events at $E_{cm}=14\,\text{GeV}$

	$\langle E_j^d\rangle$ (GeV)			$\langle E_j^e\rangle$ (GeV)		
	jet #1	#2	#3	#1	#2	#3
'3-jet' events, $E_{cm}=33\,\text{GeV}$	14.1	12.0	7.4	10.9	9.2	6.2
Jets from 2-jet events $E_{cm}=14\,\text{GeV}$		7.0			5.8	

In Fig. 8a the transverse momentum distribution of jet #3 from the 33 GeV sample is plotted together with the distribution from the 2-jet events at 14 GeV. To guide the eye the exponential fits are also drawn. The two distributions coincide. It would be premature to conclude from this that quark and gluon jets have apparently the same $p_\perp$ distributions. The fact that less than 1/3 of the solid angle is available for jet #3, whereas a jet from 2-jet events covers one hemisphere, demonstrates one different bias of the two data samples, and the $g=q$ model calculations of Fig. 8b show indeed a significantly broader distribution of the 2-jet data.

A less biased comparison is performed in Fig. 9, where only particles emitted at an angle less than 50° with respect to the jet axis are plotted. With this cut the slope of the $p_\perp$-spectrum for jet #3 is smaller than that for 2-jets and the difference observed for the $g=q$ model in Fig. 8b are largely reduced (Fig. 9b). The remaining difference between the two

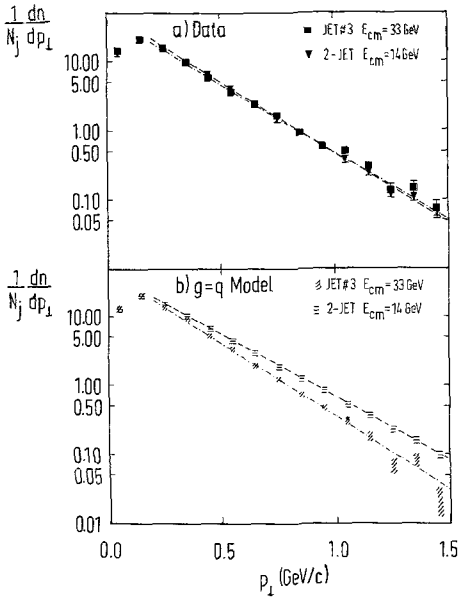

Fig. 8a and b. **a** The differential $p_\perp$-distribution of jet #3 from '3-jet' events of the 33 GeV sample together with the distribution for jets from 2-jet events at $E_{cm}=14$ GeV; **b** the same distribution as predicted by the $g=q$ model

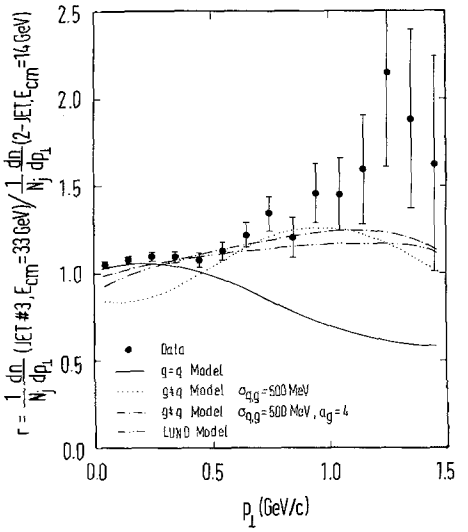

Fig. 10. The ratio of the $p_\perp$-distribution of jet #3 at $E_{cm}=33$ GeV to that of jets from 2-jet events at $E_{cm}=14$ GeV (from Fig. 9a) together with model results

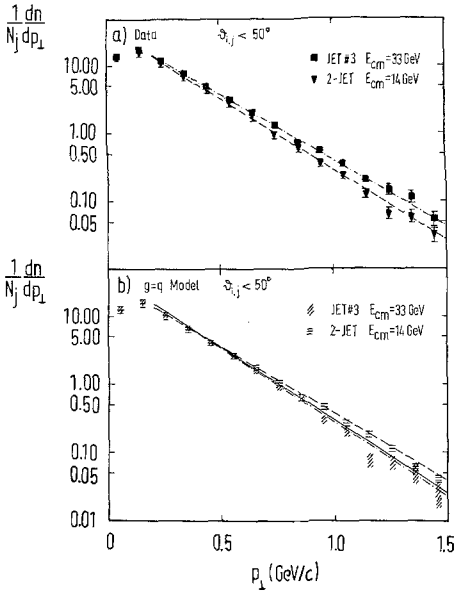

Fig. 9a and b. The differential $p_\perp$-distribution for the same events as in Fig. 8 but including only particles within a 50° cone around the jet axis

distributions in the model (Fig. 9b) is due to the fact that 2-jet events at 14 GeV already include a certain fraction of $q\bar{q}g$-events which flatten the distribution, and, that the 3-jet sample still contains a fraction of $q\bar{q}$-events. If the $g=q$ model is analyzed without this background, the two distributions agree with each other. Inclusion of 4-parton final states to the 3-jet events changes the slope of jet #3 by at most 0.1 as indicated by the full line in Fig. 9b.

In Fig. 10 the ratio of the differential $p_\perp$-distribution (Fig. 9a) of jet #3 to that of 2-jets is plotted together with several model results. The experimental ratios show an increase from 1.05 to 1.5, whereas the prediction for the $g=q$ model falls to 0.6. Taking $\sigma_{q,g}=500$ MeV results in a better agreement in the region $0.5\,\text{GeV}<p_\perp<1.0\,\text{GeV}$, but does not describe the data at low $p_\perp$. Only changing both the fragmentation function and the transverse momentum distribution for the gluon jet ($a_g=4.0$ and $\sigma_{q,g}=500$ MeV) results in a rough description of the data up to $p_\perp=1.0$ GeV. Nearly the same agreement with the data is found for the Lund model. The agreement for $p_\perp>1.0$ GeV can be improved by the inclusion of '4-parton' events.

4.2. *Average Particle Multiplicity in Jets*

Since the transverse momentum distribution of the lowest energy jet, #3, is broader than that of the other jets, one might expect differences in the multiplicity distribution, as well. For the 33 GeV sample Fig. 11a shows the observed mean multiplicity of charged particles $\langle n_{ch}\rangle$ as a function of E_j^e. The increase of $\langle n_{ch}\rangle$ with E_j^e is expected since the total multiplicity increases strongly with E_{cm}. For a given energy $\langle n_{ch}\rangle$ is, within errors, the same for all three jets.

In the models an increase of multiplicity may be

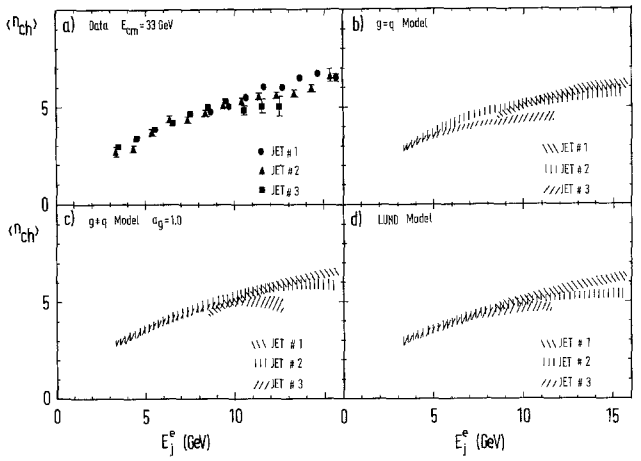

Fig. 11a–d. The average charged multiplicity as a function of E_j^e using the 33 GeV sample, **a** shows the experimental data, and **b**, **c**, **d** the different model results at $E_{cm}=33$ GeV

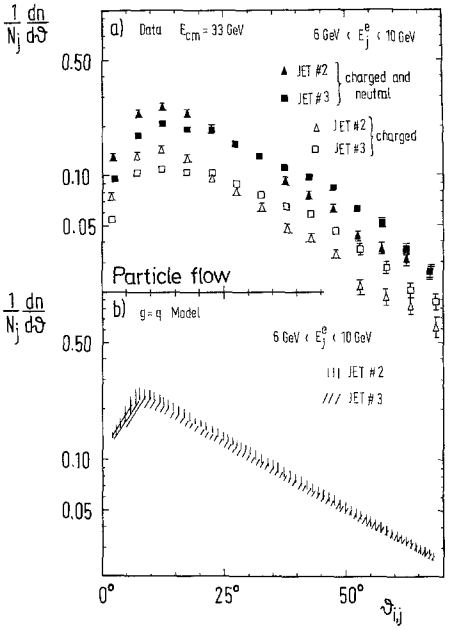

Fig. 12a and b. The averaged particle flow as a function of the angle with respect to the jet axis (particle flow). **a** data and **b** $g=q$ model at $E_{cm}=33$ GeV

achieved by increasing the parameter a, i.e. by lowering the mean energy loss per step $\langle z \rangle$. The multiplicity within a cone of 50° around the jet axis of a quark jet of 8 GeV increases from 6.6 to 7.1, respectively 7.6 for an increase of a from 0.5 to 1.0, respectively 4.0, corresponding to a decrease of $\langle z \rangle$ from 0.38 to 0.25, respectively 0.17. Furthermore, the fragmentation schemes of the models are constructed such that an increase of σ_q from 300 MeV to 500 MeV lowers the total multiplicity from 6.6 to 6.0, indicating only a weak dependence of the multiplicity on a and σ_q at these energies.

For the $g=q$ model (Fig. 11b) $\langle n_{ch} \rangle$ tends to be slightly lower for jet #3 than for #2. The model agrees quite well with the data for $a_g=1.0$, $\sigma_{q,g}=300$ MeV (Fig. 11c), or for $\sigma_{q,g}=500$ MeV and $a_g=4.0$ (not shown). There is also good agreement with the Lund model (Fig. 11d).

Similar conclusions are drawn, studying the multiplicity as a function of E_j^d for the 22+33 GeV data sample. We list in Table 3 the corresponding $\langle r_{32} \rangle$ for the multiplicities (row 3 covers charged plus neutral particles; row 4 charged particles only), together with the values resulting from the Hoyer model with different values for $\sigma_{q,g}$ and a_g, and from the Lund model. The results indicate that a softer gluon fragmentation is needed to describe the data.

Averaged over all jet energies the $\langle n \rangle$ of jet #3 from the '3-jet' sample exceeds the $\langle n \rangle$ of the jets from 2-jet events at 14 GeV by about 10‰, while in the $g=q$ model the excess only amounts to 3‰.

Though the changes in multiplicity for jet energies between 5 and 10 GeV are small, there are indications that a softer gluon fragmentation describes the data better.

4.3. *Particle and Energy Flow Within Jets*

More insight may be gained by a detailed study of the particle density within the jets. For jets with $6\,\text{GeV}<E_j^e<10\,\text{GeV}$ from the 33 GeV data sample, the observed averaged angular density of particles as a function of the angle with respect to the jet axis (particle flow) is shown in Fig. 12a (full symbols for charged and neutral particles; open symbols for charged particles only). For $\vartheta_{i,j}<25°$, where $\vartheta_{i,j}$ is the angle between the particle i and the jet axis j, the density of particles is less for jet #3 than for #2, but for $35°<\vartheta_{i,j}<60°$ the reverse is true. In the $g=q$ model (Fig. 12b) jet #3 has a particle density equal to or smaller than that of jet #2 over the whole region.

Model calculations with jets of about 8 GeV show that an increase of σ_q from 200 MeV to 600 MeV results in a decrease of the multiplicity in the region $\vartheta_{i,j}<25°$, whereas in the region $25°<\vartheta_{i,j}<50°$ the number of particles stays roughly constant. A change of one of the parameters α or β such as to soften the fragmentation increases the multiplicity mainly in the region $25°<\vartheta_{i,j}<50°$.

In Fig. 13 the experimental ratio of the particle flow of jet #3 to that of jet #2 is displayed together with several model results. The data points show an increase from 0.75 at $\vartheta_{i,j}<10°$ to 1.4 at $\vartheta_{i,j}\sim 50°$, whereas the ratio for the $g=q$ model is close to 1.0 over the entire region. Increasing $\sigma_{q,g}$ to 500 MeV decreases the ratio only for $\vartheta_{i,j}<25°$. A

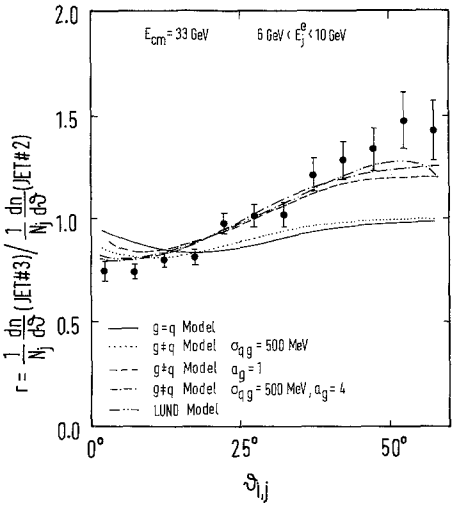

Fig. 13. The ratio of the particle flow of jet #3 to that of jet #2 together with several model results. ϑ is the angle with respect to the jet axis

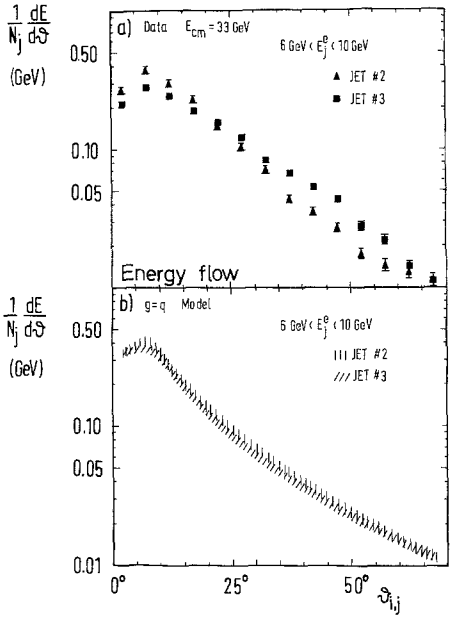

Fig. 14a and b. The average energy flow per jet with respect to the jet axis for jets #2 and #3; **a** and **b** represent, respectively the data and the $g=q$ model at $E_{cm}=33$ GeV

change of α_g from 0.5 to 1.0 leads to a better agreement in the region $25°<\vartheta_{i,j}<60°$, but spoils the agreement for the data below 10°. The dashed dotted curve ($\alpha_g=4.0$, $\sigma_{q,g}=500$ MeV) gives a rough description of the data. The same agreement with the data is seen for the Lund model.

The energy flow around the jet axis (Fig. 14a) shows a similar behavour. Jet #3 exhibits a depletion for $\vartheta_{i,j}<25°$ and an excess for $25°<\vartheta_{i,j}<60°$ relative to jet #2, whereas for the $g=q$ model

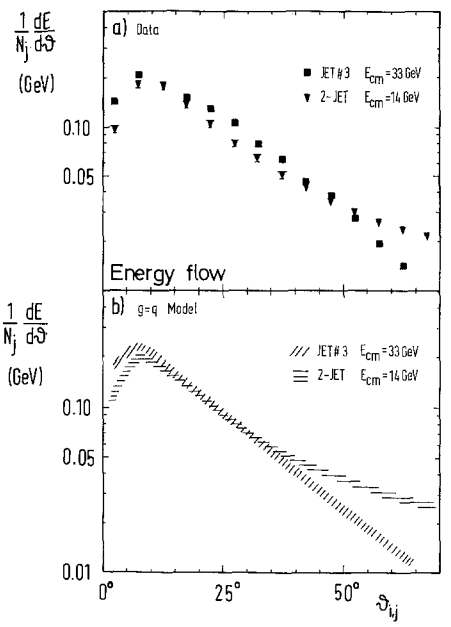

Fig. 15a and b. The average energy flow of jet #3 of the '3-jet' events together with that of jets from 2-jet events at 14 GeV; **a** represents the data and **b** the $g=q$ model

(Fig. 14b) the points of jet #3 are again on or below those of jet #2.

Similar results were obtained, for jets with $6\text{ GeV}<E_j^d<10\text{ GeV}$ of the 22+33 GeV data sample. A comparison of the energy flow of jet #3 of the '3-jet' events with that of 2-jet events at 14 GeV is given in Fig. 15a. Again an enhancement of energy flow for jet #3 in the region $25°<\vartheta_{i,j}<50°$ is visible, which is not reproduced by the $g=q$ model in Fig. 15b. For $\vartheta_{i,j}>50°$ the distribution of jet #3 drops quite rapidly in both figures, due to the fact that the solid angle available for jet #3 is more restricted than for jets of 2-jet events.

All these distributions show that for roughly the same jet energy, jet #3 has a broader particle and energy flow than jet #2 or jets from 2-jet events at $E_{cm}=14$ GeV. To obtain a reasonable description of these effects by the Hoyer model one has to enlarge $\sigma_{q,g}$ and α_g. The Lund model is in rough agreement with the data.

4.4. Longitudinal Momentum Distribution

To complete the global investigation of jets we now turn to the distribution of longitudinal momenta. We present the results in terms of the $x_{\parallel}$-distribution where $x_{\parallel}$ is defined as:

$$x_{\parallel}=p_{\parallel}/E_j \tag{11}$$

where $p_{\parallel}$ is the momentum component of a particle in jet j parallel to the jet direction $\mathbf{k}_j$ and E_j is the

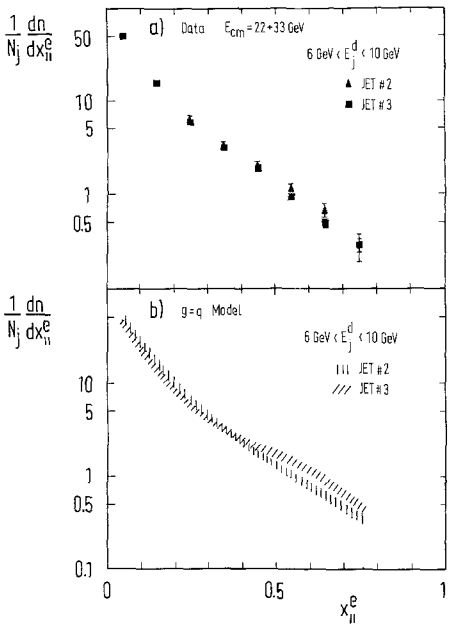

Fig. 16a and b. The differential $x_{\parallel}^e$ distribution as defined in the text for jets #2 and #3 with $6\,\text{GeV} < E_j^d < 10\,\text{GeV}$ for the 22 + 33 GeV sample; **a** represents the data and **b** the $g=q$ model

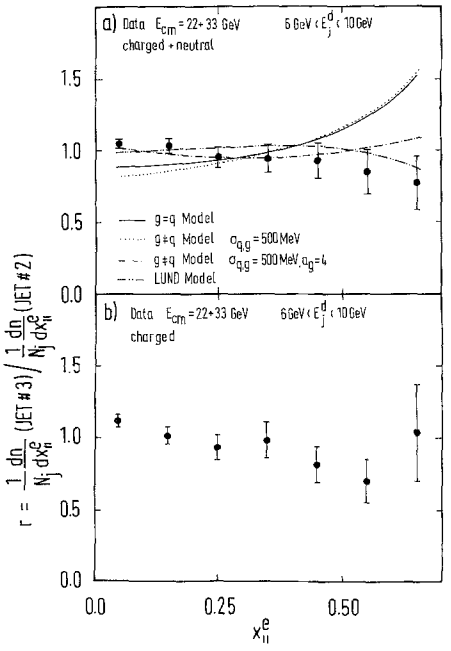

Fig. 17. a The ratio of the $x_{\parallel}^e$ distribution of jet #3 to that of jet #2 for charged and neutral particles together with model results. **b** The same ratio for charged particles only

jet energy. In the case of 3-jet events E_j has to be experimentally determined for each jet, causing considerably larger uncertainties and biases than in case of 2-jet events, where E_j is given by the beam energy. We use E_j^e for the jet energy and denote the resultant scaling variable by $x_{\parallel}^e$.

Figure 16a shows the $x_{\parallel}^e$-distribution for jets with $6\,\text{GeV} < E_j^d < 10\,\text{GeV}$ of the 22 + 33 GeV sample, for both, charged and neutral particles. Except for a slight tendency of the jet #3 points at $x_{\parallel}^e > 0.3$ to be located below those of jet #2, no significant differences are visible. In the $g=q$ model (Fig. 16b) the distribution of jet #2 falls off more steeply than that of jet #3. Which is partly an effect of the cascade decays of mesons containing c and b quarks. (Even a harder fragmentation of c and b quarks, as proposed by [14], cannot compensate for this effect.)

In Fig. 17a the ratio of the differential $x_{\parallel}^e$-distribution of jet #3 divided to that of jet #2 is plotted together with the different model results. The statistical errors are large, and the decrease of the data points with increasing $x_{\parallel}^e$ is not statistically significant. The independent fragmentation model with a softer gluon fragmentation yields a reasonable description of the data. The same is true for the Lund model.

Figure 17b shows the same ratio for the charged particle data only, demonstrating within errors the same behaviour as in Fig. 17a. Similar results are obtained, when the comparison of the data with models is repeated using the two other methods (E_j^e and the 33 GeV sample, and jet #3 with 2-jet events at $E_{cm} = 14$ GeV).

Although the measured $x_{\parallel}^e$ distribution does not permit a definite statement about differences between quark and gluon fragmentation, it is consistent with the conclusions drawn in Sect. 4.1–4.3.

4.5. *String Effect*

The particle distributions presented in the previous section were shown to be reasonably well described by both schemes, the independent parton fragmentation model of Hoyer et al. with gluon fragmentation being broader than that of quarks and by the string model of the Lund group. In this section we study whether the complete distributions of particles in an event allows to differentiate between the two models.

The two models predict different particle populations in the angular region between the jets. In the Lund model, due to the fragmentation proceeding in a different coordinate system, the region between the quark and the antiquark is depleted relative to those between the gluon and the quark or the gluon and the antiquark (see Appendix A). In a previous letter [4] we looked for such differences and found a better description of the data by the Lund model than by the Hoyer model. That analysis was based on 326 planar 3-jet events. It is repeated here with the full

statistics available at present. We further examine, whether also the particle distributions within the jets are sensitive to the different fragmentation axes used by the independent parton fragmentation scheme and by the Lund model.

Differences between the two types of models are visible in the energy flow distribution of the events. These distributions are obtained by projecting all particle momenta of an event onto the $(\mathbf{q}_2, \mathbf{q}_3)$-plane and summing the particle energies in each Θ-bin. Θ is the angle in the event plane between the particle momentum and the axis of jet #1, and runs via jets #2 and #3 back to #1. Thus the axis of jet #1 is fixed at 0°, whereas the axes of jets #2 and #3 are distributed around 155° and 230°, respectively. The differential energy flow is normalized to the total energy observed in the events. Figure 18a shows a comparison of the experimental energy flow with the two model predictions. The relative differences between the two model calculations are largest in the region between jets #1 and #2 and the data are visibly better described by the Lund model. A comparison of the 14 data points in the region $50° < \Theta < 120°$ yields $\chi^2 = 17$ for the Lund model and $\chi^2 = 42$ for the Hoyer model. The comparison of the particle flow, which includes charged and neutral particles, with the model results in Fig. 18b confirms this observation. The charged particle flow shows within the statistical errors the same distribution [15].

In the Lund model, the observed depletion of particles between jets #1 and #2 arises because $p_\perp$ is limited in the coordinate subsystems of the colour strings which, to the observer in the overall c.m. system, appears Lorentz-transformed towards the gluon hemisphere. Consequently, the differences between the two models ought to become more pronounced for particles with larger transverse mass $\sqrt{m^2 + (p_\perp^{\text{out}})^2}$, where $p_\perp^{\text{out}}$ is the momentum component normal to the event plane. In Fig. 18c, where the particle flow is plotted only for particles with $p_\perp^{\text{out}} > 0.3$ GeV/c, the differences between the two models are indeed more pronounced, and again the Lund model provides the better description of the data.

Another way to reveal these differences is to plot the distributions such that the jet axes of all events coincide. This is achieved, by plotting the particle density as a function of the normalized projected angle $\Theta_{i,j}/\Theta_{jk}$, where Θ_{jk} is the angle between the jet axes #j and #k, and $\Theta_{i,j}$ is the angle between jet axis #j and the direction of the particle i, as sketched in the upper corner of Fig. 19. The distribution is normalized to the total number of particles of the events. This density is shown in Fig. 19. Both models

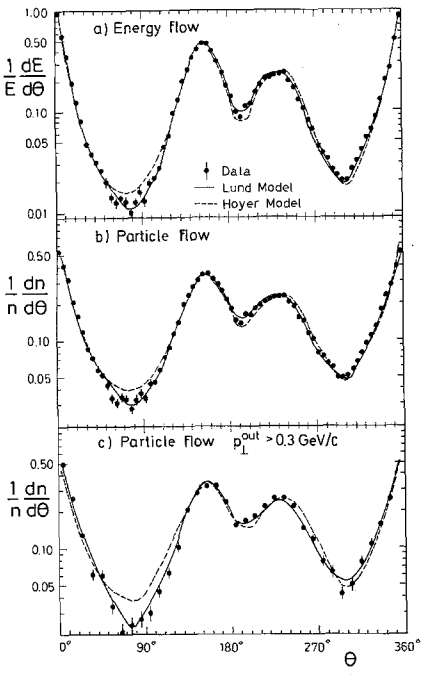

Fig. 18. a The normalized energy flow $(1/E\,dE/d\Theta)$ in the event plane $(\mathbf{q}_2, \mathbf{q}_3)$ for 3-jet events together with two model predictions. The normalized charged and neutral particle flow $(1/n\,dn/d\Theta)$ and the normalized charged and neutral particle flow $(1/n\,dn/d\Theta)$ for particles with $p_\perp^{\text{out}} > 0.3$ GeV are shown in **a** and **b** respectively. n is the total number of particles used in each plot

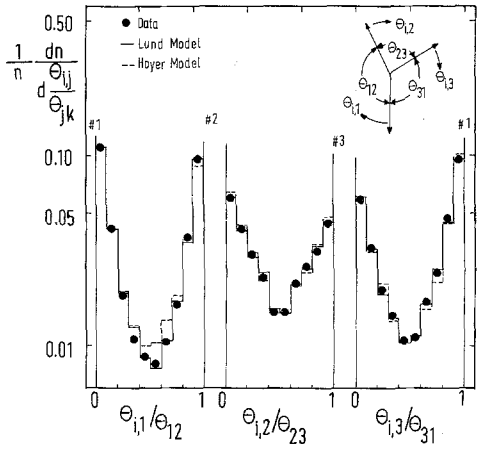

Fig. 19. The average charged and neutral particle density in the angular regions between the jet axes, normalized by the total number of particles versus $\Theta_{i,j}/\Theta_{jk}$ the data are shown together with predictions of the Hoyer and the Lund model. The definitions of $\Theta_{i,j}$ and Θ_{jk} are sketched in the right hand upper corner

describe the data well, except in the region between jet #1 and #2, where the Hoyer model predicts more particles than experimentally observed.

As a relative measure of the particle density in the region between the jets the ratio of the number

Table 5. The ratio of the number of particles in the angular range $0.3<\Theta_{i,j}/\Theta_{jk}<0.7$ between jets #1 and #3 to the corresponding number between jets #1 and #2, together with the statistical uncertainties, both for the data and the model calculations. The last line shows the corresponding ratios for the energy flow

Row		Particles	Data	Lund model	Hoyer model	
					$a_g=4.0$ $\sigma_{q,g}=500$ MeV	$g=q$
1	ratio of number particles	all	1.39 ± 0.04	1.33 ± 0.03	1.09 ± 0.03	1.03 ± 0.03
2		charged only	1.42 ± 0.06	1.27 ± 0.03	1.04 ± 0.04	1.02 ± 0.04
3		$p_\perp^{out}>0.3$ GeV/c	1.73 ± 0.13	1.55 ± 0.07	1.12 ± 0.07	0.96 ± 0.07
4		$p_\perp^{out}>0.3$ GeV/c charged only	1.82 ± 0.16	1.52 ± 0.08	1.14 ± 0.09	1.01 ± 0.09
5		K	$1.9\ \pm0.2$	$1.7\ \pm0.15$	1.14 ± 0.1	$1.0\ \pm0.1$
6	ratio of energy	all	1.56 ± 0.04	1.50 ± 0.03	1.20 ± 0.03	1.09 ± 0.03

of particles in the range $0.3<\Theta_{i,j}/\Theta_{jk}<0.7$ between jet #1 and #3 to the number between jet #1 and #2 is taken. This ratio is listed in the first two rows of Table 5, together with the model predictions. The observed behaviour persists, even if the lower momentum cut off for the particles is raised to 0.5 GeV/c. To verify that the difference between the Hoyer model and the data cannot be explained by the inclusion of '4-parton' events, the analysis was repeated taking only '4-parton' events, yielding a value of 1.13 ± 0.05 for the ratio.

The increase of the effect with higher transverse mass is quantified in rows 3 and 4 of Table 5, where the ratio is given for particles with $p_\perp^{out}>0.3$ GeV/c only. Increasing the mass by accepting only K-meson candidates, yields similar results as listed in row 5 of Table 5. For $p<0.8$ GeV/c these candidates are identified as charged kaons by the measurement of their energy loss in the central detector [16] while for $p>0.8$ GeV/c reconstructed neutral kaons [17] are used. The background of this enriched kaon sample is estimated to be about 50% for the data and the model calculations. The ratio of the energy flow for the same angular range as above is given in row 6 of Table 5.

Fragmentation along the colour-anticolour axes, provides a better description of the particle distributions not only in the angular regions between jets #1 and #2 but also within the jets. Excluding for instance the range $50°<\Theta<120°$ in the energy flow distribution (Fig. 18a) from the comparison, one still obtains $\chi^2/\text{d.f.}=2(5)$ for the Lund (Hoyer) model. A refined investigation [18] shows that at least part of this difference reflects the different fragmentation schemes. For each particle in a jet the momentum component in the $(\mathbf{q}_2,\mathbf{q}_3)$-plane transverse to the jet axis ($p_\perp^{in}$) is calculated. The sign of $p_\perp^{in}$ for each jet is defined by the insert of Fig. 20a. Figure 20 shows $\langle p_\perp^{in}\rangle$ for the data plotted as a function of $p_\parallel$, where $p_\parallel$ is the momentum component parallel to the jet axis. In the figure the point at $p_\parallel=5.5$ GeV/c includes all momenta above 5 GeV/c. Also shown are the predictions of the two models which have statistical errors less than half as those of the data*. At very low values of $p_\parallel$ the data and both models show a similar trend, in that $\langle p_\perp^{in}\rangle$ points towards the neighbouring jet separated by the larger angular distance. For $p_\parallel>2.5$ GeV/c, however, the two model predictions diverge. For the data and the Lund model $\langle p_\perp^{in}\rangle$ is positive (negative) for jet #1(#2) and increases (decreases) with increasing $p_\parallel$. This effect is not only caused by the different particle densities in the gap between jets #1 and #2. To show this, the particles in the region $50°<\Theta<120°$ were excluded for the analysis and the jet axes were redetermined. The results show the same tendency as in Fig. 20. A comparison of the data with the model prediction for the restricted sample taking the 4 points with $p_\parallel>2.5$ GeV/c yields $\chi^2=21(22)$ for jet #1(#2) in the case of the Hoyer model and $\chi^2=9(6)$ in the case of the Lund model.

This effect is qualitatively and quantitatively understood in the colour string picture. The momentum vectors of the low momentum particles in the quark and antiquark jet, due to the above Lorentz transformation, are pulled towards the gluon direction, which for the majority of the events is the direction of jet #3. This results in a slightly larger opening angle between the q and $\bar{q}$ jets than expected from independent parton fragmentation. Since the high momentum particles of the quark jets are less affected by the transformation, their average momenta tend to subtend a larger angle with jet axis #3 than the corresponding jet axes.

* The different calculations of the Hoyer model with the various parameter sets used in the previous section and also calculations of the model of Ali et al. [12] show the same results within the statistical errors

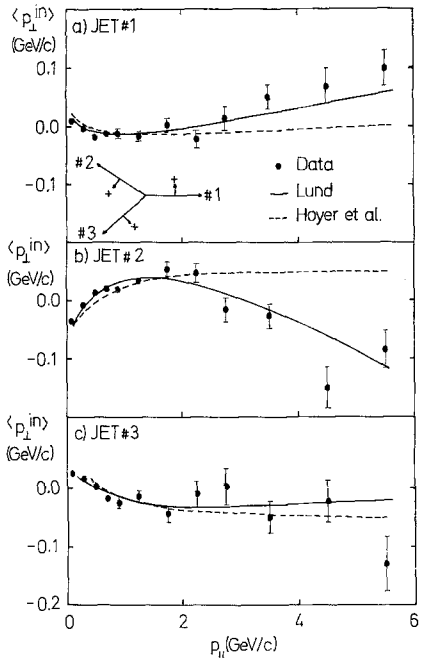

Fig. 20a–c. The average transverse momentum component in the $(\mathbf{q}_2, \mathbf{q}_3)$-plane with respect to the jet axis $\langle p_\perp^{in} \rangle$ as a function of the momentum component parallel to the jet axis for charged and neutral particles of jets #1, #2 and #3, respectively. The sign convention of $p_\perp^{in}$ is scetched as well. The predictions of the Hoyer and the Lund model are also shown

5. Summary and Conclusion

We have studied particle distributions in multihadron events produced by high energy e^+e^--annihilation. The analysis is mainly concerned with events showing 3-jet structure and with their interpretation in the framework of perturbative QCD with different fragmentation schemes.

The distributions of the transverse and longitudinal momenta in the various jets with respect to the jet axes were presented as a function of the jet energy, as well as the average particle multiplicity of these jets and the particle and energy flow distributions.

A comparison of the transverse momentum distribution has shown that the average value $\langle p_\perp \rangle$ of the lowest energy jet in 3-jet events is significantly larger than that of the other two jets at similar jet energies. QCD model calculations show that the lowest energy jet is preferentially produced by the gluon and that the observed $p_\perp$ behaviour of the data can be described if the gluon fragmentation is assumed to be broader than the one of quarks. A study of the particle and energy flow leads to a similar conclusion. For independent parton fragmentation, parametrized according to Field and Feynman one needs a $\sigma_q \approx 300$ MeV and $a \approx 0.5$ for quark jets, and $\sigma_q \approx 500$ MeV and $a \approx 4.0$ for gluon jets to describe the data, if the remaining fragmentation parameters are kept constant. This observation is corroborated by a comparison of the lowest energy jet with jets of similar average energy from 2-jet events, which are dominantly quark jets. It is also observed that the string model of the Lund group, in which by definition the gluon fragments softer than quarks, describes the data.

A detailed study was performed of distributions which are sensitive to differences between independent parton fragmentation scheme and the Lund string model, i.e. the distribution of particles between the jets and its dependence on the transverse mass $\sqrt{m^2+(p_\perp^{out})^2}$ as well as the dependence of $\langle p_\perp^{in} \rangle$ on the longitudinal momentum components of the particles in jet direction. Although the observed differences between the two schemes are small, the data favour the string model predictions of the Lund group in which the fragmentation proceeds along the colour axes.

Acknowledgement. We acknowledge the efforts of the PETRA machine group, who provided us with the opportunity of doing this experiment, and also the efforts of the technical support groups of participating institutes in the construction and maintenance of our apparatus. This experiment was supported by the Bundesministerium für Forschung und Technologie, by the Education Ministry of Japan, and by the U.K. Science and Engineering Research Council through the Rutherford Appleton Laboratory. The visiting groups at DESY wish to thank the DESY directorate for their hospitality.

Appendix A

In the Hoyer model the fragmentation occurs along the parton direction i.e. along a direction fixed in the laboratory. In contrast to this, in the Lund model the fragmentation occurs along the colour flux lines, connecting $q(\bar{q})$ and gluon, i.e. along a direction moving in the laboratory. The effect of this is shown by the following (simplified) consideration:

Assume both quarks and gluons moving with a velocity $\beta=1$ in the laboratory. One colour string then moves along the x-direction in Fig. 21a with velocity $\beta=\cos(\vartheta_{qg}/2)$.

Neglecting for the moment transverse momenta ($\sigma_q=0$), the momenta of the hadrons produced in fragmentation are given in the moving system S' (Fig. 21a) by

$$\mathbf{p}' = \{0, p'_y, 0\}. \tag{A1}$$

In the laboratory-system S we obtain

$$p_x = \gamma\beta E' = \beta\gamma\sqrt{p_y^2+m^2}$$
$$p_y = p'_y = p'. \tag{A2}$$

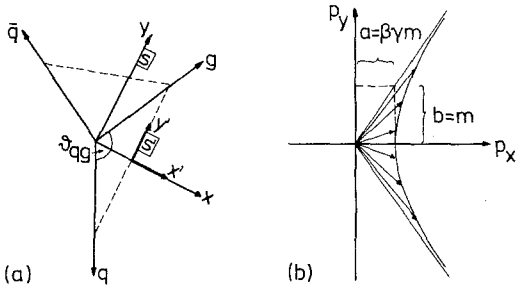

Fig. 21. a Reference frames for Lorentz transformation of fragmentation along the colour-string between quark and gluon. **b** Distribution of hadrons in momentum space (laboratory system) for $\sigma_q=0$ respectively

The momenta of particles are distributed along a hyperbola in momentum space (Fig. 21b):

$$\frac{p_x^2}{\beta^2\gamma^2 m^2}-\frac{p_y^2}{m^2}=1. \tag{A3}$$

The directions of the asymptotes are the parton directions: $b/a=1/\beta\gamma=\mathrm{tg}(\vartheta_{qg}/2)$. The distance of the hyperbola from the point $p_x=p_y=0$ increases with increasing mass (Fig. 21b). Consequently, without transverse momenta produced during fragmentation, hadrons are found in the angular intervalls between quark (antiquark) and gluon while the angular range between quark and antiquark remains empty. This phenomenon is called 'string effect'.

Transverse momenta ($\sigma_q\neq 0$) have the following effect: $p'_x\neq 0$ produces a smearing of the hyperbola (Fig. 21b) in the x, y-plane, and hadrons will be found in the previously empty intervall between quark and antiquark, i.e. the string effect is partially obscured. A transverse momentum out of the event plane, $p'_z=p_z=p_\perp^{\mathrm{out}}\neq 0$ results in an enhancement of the string effect: in (A2) and (A3) m is replaced by the transverse mass $\sqrt{(p_\perp^{\mathrm{out}})^2+m^2}$.

References

1. JADE Collab. W. Bartel et al.: Phys. Lett. **91**B, 142 (1980); MARK J. Collab. D.P. Barber et al.: Phys. Rev. Lett. **43**, 830 (1979); PLUTO Collab. Ch. Berger et al.: Phys. Lett. **86**B, 418 (1979); TASSO Collab. R. Brandelik et al.: Phys. Lett. **86**B, 243 (1979)
2. JADE Collab. W. Bartel et al.: Phys. Lett. **115**B, 338 (1982)
3. M.B. Einhorn, B.G. Weeks: Nucl. Phys. B**146**, 445 (1978); K. Shizuya, S.-H-H. TYe: Phys. Rev. Lett. **41**, 787 (1978)
4. JADE Collab. W. Bartel et al.: Phys. Lett. **101**B, 129 (1981)
5. JADE Collab. W. Bartel et al.: Phys. Lett. **123**B, 460 (1983)
6. JADE Collab. W. Bartel et al.: Phys. Lett. **88**B, 171 (1979)
7. S. Brandt, H. Dahmen: Z. Phys. C - Particles and Fields **1**, 61 (1979); S.L. Wu, G. Zobernig: Z. Phys. C - Particles and Fields **2**, 107 (1979)
8. JADE Collab. W. Bartel et al.: Phys. Lett. **119**B, 239 (1982)
9. P. Hoyer et al.: Nucl. Phys. B**161**, 349 (1979)
10. D. Field, R.P. Feynman: Nucl. Phys. B**136**, 1 (1978)
11. B. Andersson, G. Gustafson, C. Peterson: Z. Phys. C - Particles and Fields **1**, 105 (1978); B. Andersson, G. Gustafson: Z. Phys. C - Particles and Fields **3**, 223 (1980); B. Andersson, G. Gustafson, T. Sjöstrand: Z. Phys. C - Particles and Fields **6**, 235 (1980); B. Andersson, G. Gustafson, T. Sjöstrand: Phys. Lett. **94**B, 211 (1980); T. Sjöstrand: Comput. Phys. Comm. **27**, 243 (1982)
12. A. Ali, E. Pietarinen, G. Kramer, J. Willrodt: Phys. Lett. **93**B, 155 (1980); A. Ali: Phys. Lett. **110**B, 67 (1982)
13. F.A. Behrends, R. Kleiss: Nucl. Phys. B**178**, 141 (1981)
14. C. Peterson, D. Schlatter, I. Schmitt, P.M. Zerwas: SLAC-PUP-2912 (1982), submitted to Phys. Rev. D.
15. JADE Collab. W. Bartel et al.: DESY 83-079 (1983), to be submitted to Phys. Lett.
16. JADE Collab. W. Bartel et al.: Z. Phys. C - Particles and Fields **6**, 296 (1980)
17. JADE Collab. W. Bartel et al.: Z. Phys. C - Particles and Fields **20**, 187 (1983)
18. T. Sjöstrand: Private communication